ACS Photonics

pubs.acs.org/journal/apchd5

Article

Experimental Demonstration of Multidimensional and Multifunctional Metalenses Based on Photonic Spin Hall Effect

Renchao Jin, Lili Tang, Jiaqi Li, Jin Wang, Qianjin Wang, Yongmin Liu,* and Zheng-Gao Dong*

Cite This: *ACS Photonics* 2020, 7, 512−518

Read Online

ACCESS | Metrics & More | Article Recommendations | Supporting Information

ABSTRACT: Metalens is one kind of two-dimensional ultrathin lenses with subwavelength artificial structures that can focus light in a compact, flexible way. However, most strategies for designing metalenses only work on one specific spin state of light (i.e., either right- or left-circularly polarized light), hindering simultaneous control of both spins. Utilizing both the Pancharatnam-Berry phase and the propagation phase, we can rationally control the phase for each spin state of light. As proof-of-concept demonstrations, here we numerically and experimentally realize the independent focusing and manipulation of both spins of light by V-antenna metasurfaces, which can be regarded as the demonstration of the photonic spin Hall effect. Our multidimensional metalens is able to focus light of different spins at designated positions along both transverse and longitudinal directions. It can be used as a polarization analyzer to distinguish the polarization state of incident light. In addition, our multifunctional metalens can act either as a convex lens or an axicon, depending on the spin of light. The demonstrated multidimensional and multifunctional metalens has versatile potentials in spin-dependent nanophotonics, ranging from optical imaging and micro/nano-object manipulation to optical sensing.

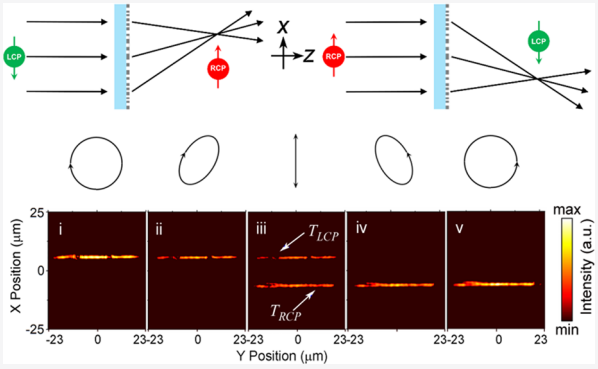

KEYWORDS: *metasurface, multifunctional lens, photonic spin Hall effect, propagation phase, Pancharatnam-Berry phase*

Metasurfaces, one emerging platform that allows us to flexibly manipulate light at nanoscales,[1,2] are composed of arrays of subwavelength meta-atoms to interact with incident light in a prescribed manner. Various optical functional components can be realized by suitably designed metasurfaces, including information encoders,[3] spin selective holograms,[4,5] vortex beam generators,[6,7] convex lenses,[8−11] axicons,[12,13] and polarization-selective devices,[14,15] which have advantages of substantial reduction in thickness, size, and complexity compared with the traditional counterparts. Metalenses can focus incident light via judicious arrangement of meta-atoms on a flat surface for wavefront shaping like a conventional lens. In contrast to the phase engineering mechanism of a conventional lens, that is, accumulating phase by varying the spatial profile of the refractive index, material thickness, or surface curvature, metalenses may modulate the phase together with the amplitude and polarization of light by the subwavelength meta-atoms.[16] Compared with conventional bulky lenses, compact metalenses show potential for integrated nano-optical applications.[1] For instance, achromatic metalenses have recently been demonstrated in the visible range, while their small size may limit their applications.[8,17,18] Researchers have also reported longitudinal multifocal metalenses.[19,20] Simultaneous focusing for two beams of different wavelengths was realized by one metalens or multilayer noninteracting metalenses.[21−23] Interestingly, metalenses with the polarization-selective function could split cross-polarization components of a linearly polarized light and focus them at different positions.[14,15] All these works indicate that metalenses exhibit some unique properties compared with conventional lenses.

Metalenses with circular-polarization sensitivity have attracted wide attention because of the manifestation of the so-called photonic spin Hall effect (PSHE) involved in such specific devices.[4,15,24−33] PSHE refers to the phenomenon that light is split into separate trajectories for different spin states, that is, left-circularly polarized (LCP) and right-circularly polarized (RCP) light.[15,23,29,30] Metasurfaces can exhibit distinct PSHE by utilizing the Pancharatnam-Berry (PB) phase. They can spatially split LCP and RCP states of light with anomalous reflection or refraction angles. However, the different reflection/refraction angles generated by the PB phase hinder metalenses to realize simultaneous focusing of different spin states. For example, the hyperbolic phase designed for a convex metalens is valid for only one spin state of light, but not

Received: November 8, 2019
Published: January 16, 2020

https://dx.doi.org/10.1021/acsphotonics.9b01608
ACS Photonics 2020, 7, 512−518

the other. Therefore, such a metalens has a real focus for LCP (or RCP) light and a virtual focus for RCP (or LCP) light. In other words, it acts as a convex lens for LCP (or RCP) light, but a concave lens for RCP (or LCP) light.[9,34] To circumvent this limitation, recently, an integration method of optical metalens and conventional convex lens has been proposed, leading to PSHE-based focusing for both spin states of light.[35,36] However, the overall size of such a combined lens is large and not suitable for device integration. So far, it still remains challenging to realize a highly miniaturized, PSHE-based focusing lens for arbitrary optical spins by an ultrathin metasurface.

Recent progress in metasurfaces opens up a new route to simultaneously control LCP and RCP light with independent modulation of propagation and PB phases.[4,25−29] It is well-known that the propagation phase is related to the geometric parameters of meta-atoms and is spin-independent, while the PB phase is related to the rotation angles of meta-atoms and imparts opposite phases to LCP and RCP light. Taking advantage of these properties, we could convert arbitrary spin angular momentum into orbital angular momentum.[25] Moreover, chiral metasurface holograms characterized by fully independent far fields of LCP or RCP light were reported.[4,5] In this paper, we develop a design method to realize multidimensional and multifunctional PSHE-based metalenses for light with arbitrary optical spin states, which have not been demonstrated numerically or experimentally. Here, multidimensional manipulation means that the metalens can separately focus light of different spins either along the longitudinal or the transverse direction, while multifunctional manipulation means that the metalens can simultaneously function as a convex lens and an axicon, depending on the spins of light. Such novel metalenses are expected to have many important applications, including but not limited to polarimetric imaging, micro/nano-object manipulation, and optical sensors.

METHOD AND RESULTS

Figure 1 shows a schematic diagram of the proposed metalens. For LCP light, the metalens efficiently converts its spin state to RCP light and focuses it at location $x > 0$ as shown in Figure 1a. In contrast, RCP incident light will be efficiently converted to LCP light and focused at the location $x < 0$ (Figure 1b). Figure 1c presents that the metalens has a combined phase that is a summation of propagation and PB phases. By synthetic modulation of the two phases, independent controls for LCP and RCP light can be achieved, which lead to the transversely focused beams along the x direction. Note that the designed metalens is a cylindrical lens (i.e., focusing the incident light into a line along the y-axis, rather than a point focusing), because the meta-atoms are periodically arranged along the y direction for simplification in nanofabrication.

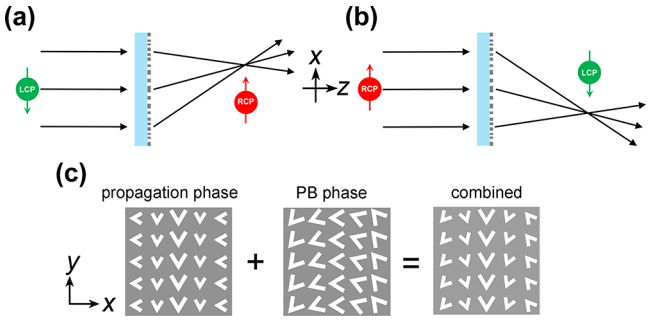

Figure 1. (a) Schematic of the metalens for the LCP incident light. (b) Schematic of the metalens for the RCP incident light. (C) Relationship between propagation, PB, and combined phases.

The meta-atom used in our metalens design is a V-shaped aperture etched through a 40 nm thick silver film, as illustrated in Figure 2a. It has an opening angle 60°, arm width b = 100 nm, and a varying arm length a. The meta-atoms are arranged with a periodicity p = 500 nm to construct the metalens. Note that the PB phase imposes an external phase on circularly polarized light given by $\varphi_{LCP/RCP} = 2\sigma\theta$, where θ is the rotation angle of meta-atoms and $\sigma = \pm 1$ for LCP and RCP incident light, respectively.[24] That is to say, PB phase can ensure a phase modulation from 0° to ±360° as the rotation angle varies from 0° to 180°. On the other hand, a full modulation of the propagation phase from 0° to 360° is also preferred in order to realize the complete and independent phase control for LCP and RCP light. Figure 2b shows the numerically calculated propagation phase and transmit amplitude of light at the wavelength of 1064 nm with arm length a varying from 270 to 460 nm for two meta-atoms: V0 (θ = 0°) corresponds to the case that the opening of V points to the right, while V90 (θ = 90°) corresponds to the case that the opening of V points upward. In the simulation, the incident light is circularly polarized, and the phase and amplitude are probed for the transmitted light with the opposite spin state. Note that the propagation phase and amplitude for one specific meta-atom are independent of the optical spin of the incident beam. The numerical simulation results show that the V-shaped apertures can lead to full modulation of the propagation phase, since V0 covers propagation phase ranging from 0° to 180°, while V90 covers from 180° to 360°. Equally importantly, the amplitude

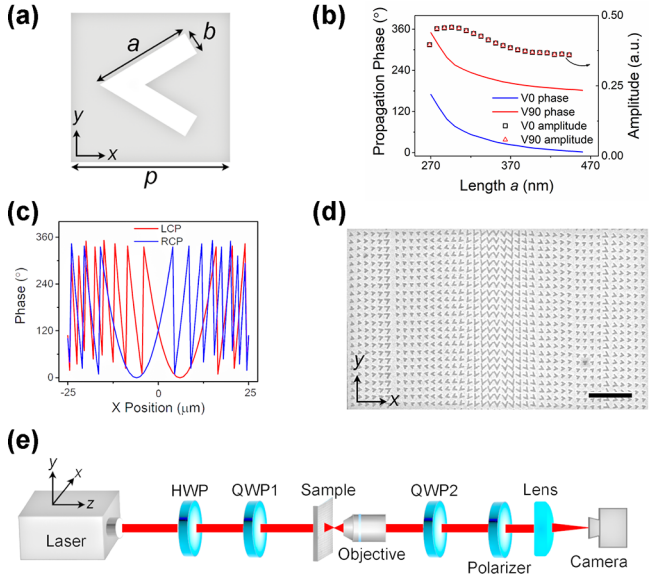

Figure 2. (a) Parameters of the V-shaped apertures. (b) Propagation phase and amplitude (normalized to the incident electric field of 1 V/m) of V-shaped apertures with length a varying from 270 to 460 nm. (c) Phase requirement for the designed PSHE-based metalens. (d) SEM image of the fabricated metalens. Scale bar 3 μm. (e) Schematic of the optical setup for measurement.

https://dx.doi.org/10.1021/acsphotonics.9b01608
ACS Photonics 2020, 7, 512−518

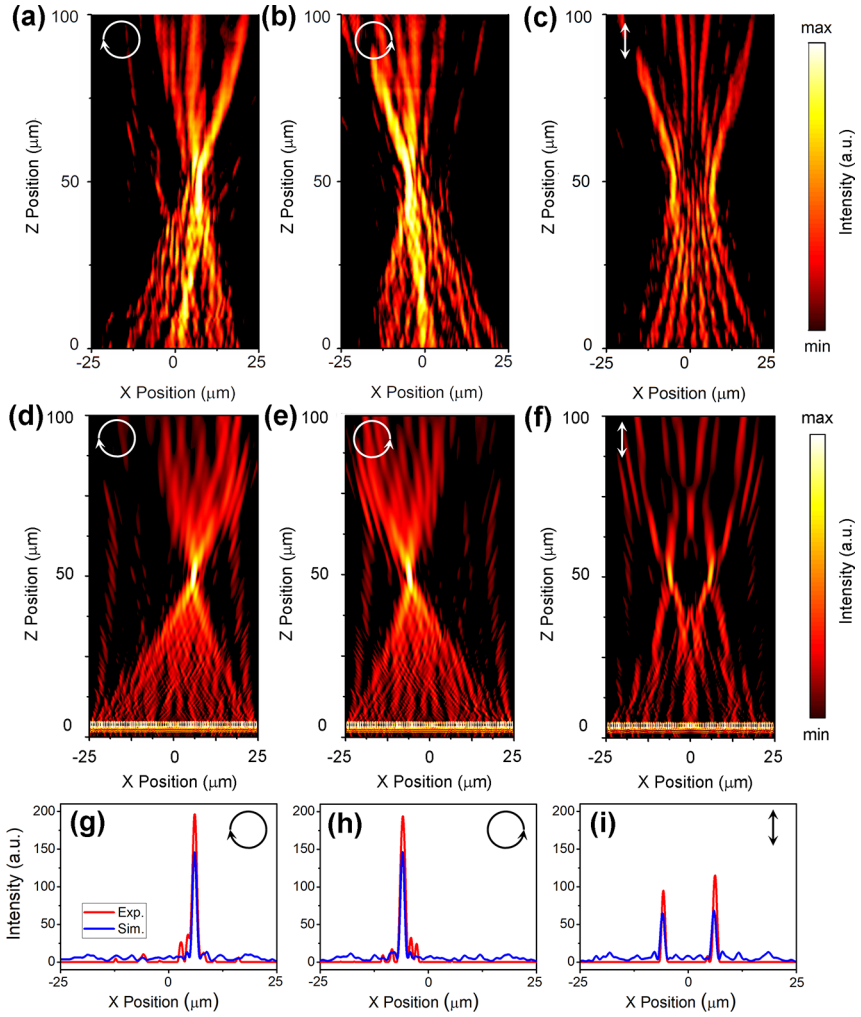

Figure 3. (a–c) Measured intensity distribution of PSHE-based metalens for LCP, RCP, and LP incidences, respectively. (d–f) Simulated optical images for LCP, RCP, and LP incidences, respectively. (g–i) Transverse intensity distribution in the focal plane for LCP, RCP, and LP incidences, respectively. (a)–(f) are plotted in the logarithmic scale.

of transmission can maintain on a same level around 0.4 for V0 or V90 antennas with varying lengths.

As a proof-of-concept demonstration of the PSHE-based focusing phenomenon, we have designed a cylindrical metalens that requires different hyperbolic phase profiles for LCP and RCP light given by[23]

$$\varphi_{\mathrm{LCP}}(x) = \frac{360^\circ}{\lambda}\left(\sqrt{(x-\Delta x)^2 + f^2} - f\right) \tag{1}$$

$$\varphi_{\mathrm{RCP}}(x) = \frac{360^\circ}{\lambda}\left(\sqrt{(x+\Delta x)^2 + f^2} - f\right) \tag{2}$$

Here, f is the designed focal length of the cylindrical metalens, λ is the wavelength in free space (1064 nm for this work), Δx is the transverse offset of the focal line from the center ($x = 0$). In our specific design, we consider the focal length $f = 50$ μm and transverse offset $\Delta x = 6$ μm. The phase distributions along the x direction can be obtained from eqs 1 and 2, which are plotted in Figure 2c.

We use propagating phase (ϕ^{Pro}) and PB phase (ϕ^{PB}) to achieve the required phase profile. Considering that

$$\varphi_{\mathrm{LCP}}(x) = \phi^{\mathrm{Pro}}_{\mathrm{LCP}}(x) + \phi^{\mathrm{PB}}_{\mathrm{LCP}}(x) \tag{3}$$

$$\varphi_{\mathrm{RCP}}(x) = \phi^{\mathrm{Pro}}_{\mathrm{RCP}}(x) + \phi^{\mathrm{PB}}_{\mathrm{RCP}}(x) \tag{4}$$

and reminding that

$$\phi^{\mathrm{Pro}}_{\mathrm{LCP}}(x) = \phi^{\mathrm{Pro}}_{\mathrm{RCP}}(x) = \phi^{\mathrm{Pro}}(x) \tag{5}$$

$$\phi^{\mathrm{PB}}_{\mathrm{LCP}}(x) = -\phi^{\mathrm{PB}}_{\mathrm{RCP}}(x) = 2\theta(x) \tag{6}$$

we can get

$$\phi^{\mathrm{Pro}}(x) = \frac{\varphi_{\mathrm{LCP}}(x) + \varphi_{\mathrm{RCP}}(x)}{2} \tag{7}$$

$$\theta(x) = \frac{\varphi_{\mathrm{LCP}}(x) - \varphi_{\mathrm{RCP}}(x)}{4} \tag{8}$$

Equations 7 and 8 are the design requirements for the transverse phase of the PSHE-based metalens, which can be readily retrieved from the phase profiles shown in Figure 2c. Therefore, we can determine the arm lengths $a(x)$, according to Figure 2b, as well as the rotation angles $\theta(x)$ for all meta-atoms at different positions. The designed metalens was fabricated by the following steps. First, a chromium film with 2 nm in thickness was sputtered on a glass substrate to server as the adhesion layer, followed by the deposition of a 40 nm-thick

https://dx.doi.org/10.1021/acsphotonics.9b01608
ACS Photonics 2020, 7, 512–518

silver film. Then, the 40 nm thick silver film was etched by a focus ion beam system (FEI, FIB 200) with an ion current of 35 pA and voltage of 30 kV. The scanning electron micrograph of the fabricated sample is shown in Figure 2d. The entire metalens has an area of 50 × 45 μm^2.

We have experimentally characterized the performance of the PSHE-based cylindrical metalens by the setup schematically presented in Figure 2e. The sample is mounted on a motorized positioning system. A collimated laser beam at the wavelength of 1064 nm is incident on the backside of the sample. A half-wave plate (HWP) is used to adjust linear polarization of the incident beam. The orthogonal circular-polarization states, between the incident beam impinging onto the sample and the transmitted light collected by a 50× (NA 0.75) objective for camera imaging, are guaranteed by rotating two quarter-wave plates (QWP1 and QWP2) synchronously. The polarizer before the camera ensures that the linear polarization of the light collected by the camera is perpendicular to that of the incident beam.

Figure 3a–c shows the measured optical microscopy images for three polarization states of incident light, corresponding to LCP, RCP, and linear polarization (LP), respectively. As shown in Figure 3a, for the LCP beam, we observe a single focal spot along the z axis that is parallel to the incident path. Both the measured focal length f = 50 μm and transverse offset x = +6 μm agree well with the designed parameters. Figure 3b shows the measured focusing image for RCP incidence. We can also observe a single focal spot with the same focal length of f = 50 μm but an opposite transverse offset of x = −6 μm, nicely matching our original design. It is well-known that LP light can be regarded as a superposition of LCP and RCP light. Therefore, the focusing image for LP in Figure 3c has two focal spots with the identical focal length of f = 50 μm, but opposite transverse offsets at x = ±6 μm simultaneously. The split focusing behavior for beams with different spins manifests the significant PSHE from our metalens. To provide a better understanding of the PSHE-based metalens, we have performed numerical simulations by the finite-difference time-domain method. The results are shown in Figure 3d–f. It is clear that simulation results in Figure 3d–f agree quite well with the measured optical images in Figure 3a–c, respectively. The differences between measurement and simulation are mainly due to the imperfect sample fabrication. In addition, we compare the measured and simulated intensity distribution along the x axis in focal plane z = 50 μm for LCP, RCP, and LP incidence, as shown in Figures 3g–i, respectively. From Figure 3g, the full-width at half-maximum (FWHM) of the focal point for LCP is 1.08 μm in experiment and is 1.13 μm in simulation. These results are in good agreement with the theoretical values considering the numerical aperture ($NA = \frac{r}{\sqrt{r^2+f^2}} = 0.45$, r is the width of metalens) of the metalens. For RCP light in Figure 3h, the FWHM is 1.2 μm in measurement and 1.1 μm in simulation. As for the LP incident light in Figure 3i, both the left and right focal points exhibit an FWHM of 0.96 μm in measurement and 1.14 μm in simulation.

From simulations, our multidimensional metalens (and other devices shown in the following) can work well from 1000 to 1100 nm (Supporting Information, Figure S1), with a transmission efficiency of 16% in simulation and 10% at the wavelength of 1064 nm in experiment (Supporting Information, Figure S2). The relatively low efficiency is mainly due to the Ohmic loss of the metallic structures used in the current design. The efficiency could be further improved by optimizing the geometries, using multilayered metallic antennas or employing dielectric structures.

Since our PSHE-based metalens is sensitive to the polarization of incident light, it can be used as a polarization analyzer[37] based on the fact that all polarizations of light can be regarded as the superposition of LCP and RCP light. The properties of our PSHE-based metalens with the identical position of focal plane and concentrated light for each spin state of incident light are beneficial for implementing highly compact polarization analyzers. In our experiment, we can achieve arbitrary polarization of incident light by rotating QWP1 in front of the laser. Then the energy of light of arbitrary polarization can be decomposed into two components[25]

$$P(\alpha) = \cos^2(\alpha)P_L + \sin^2(\alpha)P_R \quad (9)$$

where α is the rotation angle of QWP1 that determines the polarization state of incident light. The first term in eq 9 represents the intensity of the LCP component of the incident light that will be focused at the position x = +6 μm in the focal plane. Similarly, the second term represents the intensity of the RCP component of the incident light that will be focused at the position x = −6 μm. Accordingly, we can find out α by comparing the measured maximum intensities on positions x = +6 μm and −6 μm in the focal plane, and thus, the metalens can distinguish any polarization state of the incident light. Figure 4a shows intensity mapping in the focal plane for five

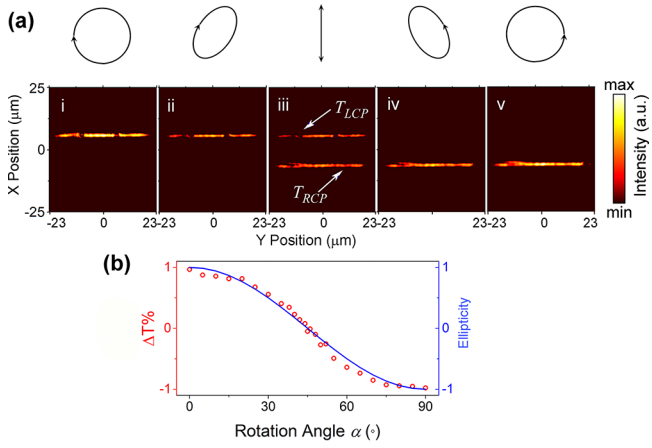

Figure 4. (a) Optical images in the focal plane of PSHE-based metalens for incident light with different polarizations. From panel i to panel v, the rotation angle of QWP1 is 0°, 30°, 45°, 60°, and 90°, labeled as LCP, EP1, LP, EP2, and RCP, respectively. The intensity is plotted in logarithmic scale. (b) Intensity difference ratio between two focusing lines versus rotation angle of QWP1, corresponding to the ellipticity of incident light.

polarization states of incident light. Clearly, the focusing intensity at position x = +6 μm (T_{LCP}) decreases, while another focusing intensity at x = −6 μm (T_{RCP}) increases as the incident polarization changes by rotating α from 0°, 30°, 45°, 60° to 90°, labeled as LCP, EP1, LP, EP2, and RCP, respectively. The measured intensity difference ratio $\Delta T\% = (T_{LCP} - T_{RCP})/(T_{LCP} + T_{RCP})$, corresponding to the ellipticity of incident light, is plotted in Figure 4b (red circles). It shows very good agreement with the theoretical curve (blue line)

https://dx.doi.org/10.1021/acsphotonics.9b01608
ACS Photonics 2020, 7, 512–518

calculated by eq 9, confirming that our PSHE-based metalens can be used as an ultrathin polarization analyzer.

In addition to the transverse focusing, a longitudinally split bifocus metalens is also designed according to eqs 7 and 8, demonstrating that our method can realize multidimensional focusing manipulation. In the design, we set $\Delta x = 0$ μm, $f_{LCP} = 50$ μm and $f_{RCP} = 35$ μm in eqs 1 and 2. Hence, the LCP and RCP light at the wavelength of 1064 nm will show different focal lengths after transmitting through the PSHE-based metalens. The SEM image of this metalens is presented in Figure 5a. As shown in Figure 5b, the transmitted light for LCP

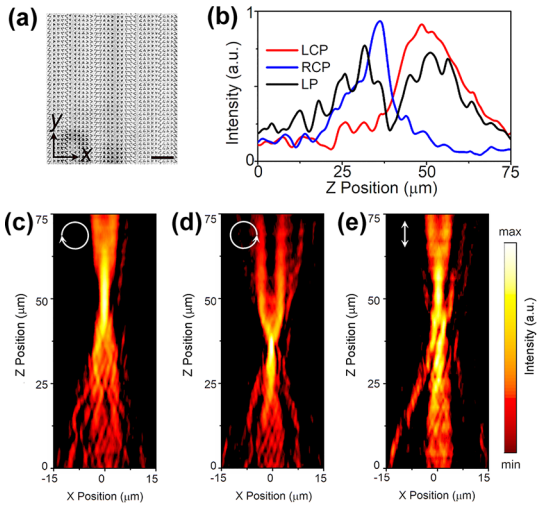

Figure 5. (a) SEM image of the longitudinally split bifocus metalens. Scale bar 3 μm. (b) Measured intensity distribution versus z position at $x = 0$ μm. (c–e) Measured intensity distribution of the multidimensional metalens for LCP, RCP, and LP incidences, respectively. The intensity is plotted in logarithmic scale.

incidence is experimentally focused at position $z = 49$ μm. For RCP incidence, a focal point located at position $z = 36$ μm is experimentally found in Figure 5c. In addition, for LP, the transmitted light exhibits focusing positions of both (Figure 5d). We plot the longitudinal intensity distribution for $x = 0$ μm for LCP, RCP, and LP in Figure 5e for a better comparison. The results show that the developed method can be used to realize transverse, as well as longitudinal, spin-sensitive focusing, so-called multidimensional manipulation by our PSHE-based metalens.

Finally, to achieve multifunctional manipulation of light by the PSHE-based metalens, we experimentally demonstrate a metalens working as an axicons for LCP light but a convex lens for RCP. In contrast to the multidimensional metalens demonstrated earlier as a cylindrical lens (i.e., only one-dimensional phase gradient modulation along the x axis but not along the y axis), the multifunctional metalens is designed to be of two-dimensional phase gradient modulation, so that we can expect a better Bessel-beam demonstration of axicons. The SEM image of fabricated multifunctional PSHE-based metalens is presented in Figure 6a, with a metasurface size of 14×14 μm^2. The designed function of convex lens for RCP light is set to have a focal length of $f_{RCP} = 30$ μm, while the axicons designed for LCP light is to generate the Bessel beam with the phase distribution given by[12,38]

$$\varphi'_{LCP}(x, y) = \frac{360^\circ}{\lambda}\sqrt{x^2 + y^2}\cdot \mathrm{NA} \tag{10}$$

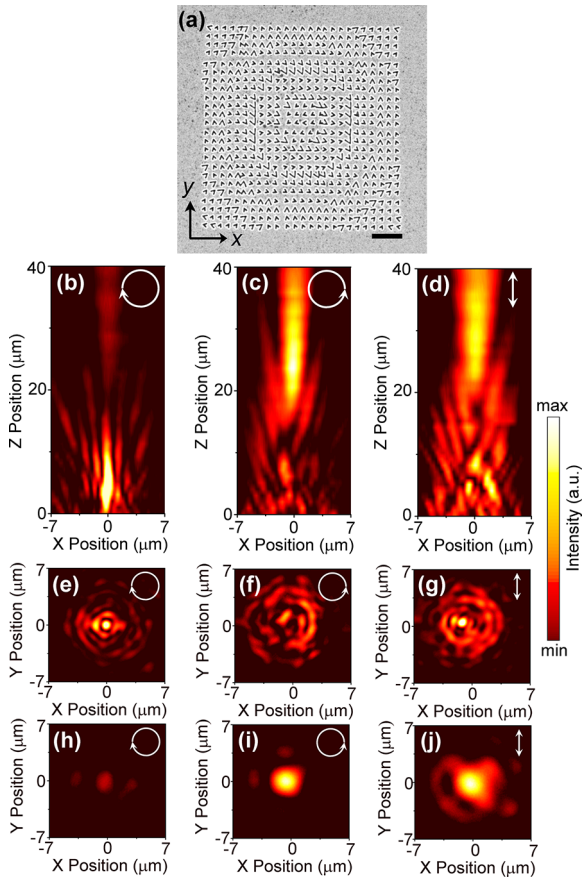

Figure 6. (a) SEM image of the multifunctional PSHE-based multifunctional metalens. Scale bar 2 μm. (b–d) Optical images of measured intensity in the x–z plane ($y = 0$ μm) for LCP, RCP, and LP incidences, respectively. (e–g) Optical images of measured intensity in the x–y plane ($z = 8$ μm) for LCP, RCP, and LP incidences, respectively. (h–j) Optical images of measured intensity in the x–y plane ($z = 30$ μm) for LCP, RCP, and LP incidences, respectively. (b)–(j) are plotted in logarithmic scale.

where the NA of designed axicons is set to be 0.5. Figure 6b–j depicts the measured results for the multifunctional metalens. Obviously, the function of axicons is realized for LCP incidence, producing a nondiffracting Bessel beam from $z = 3$ to 12 μm, as shown in Figure 6b. The measured xy-plane intensity at position $z = 8$ μm (Figure 6e) matches the intensity profile of a zero-order Bessel beam and there is no obvious intensity distribution at position $z = 30$ μm (Figure 6h). For the RCP incidence, we can experimentally observe a focal point at $z = 25$ μm as demonstrated in Figure 6c. The difference between the measured focal point and the expected one is caused by the fabrication imperfection and small size of our multifunctional metalens. From Figure 6f, we can see that no Bessel beam exists at position $z = 8$ μm for RCP incidence. However, in the focal plane $z = 30$ μm for RCP incidence, a single bright point is observed, as shown in Figure 6i, which proves its function as a convex lens rather than an axicons. Moreover, we have measured intensities for LP incidences as plotted in Figure 6d, g, and j. The light intensity in the plane $z = 8$ μm (Figure 6g) shows Bessel-like beam shape and a focus point is observed at the position $z = 30$ μm (Figure 6j). However, the intensity distribution is somewhat irregular because the interference of the focal point for RCP from the Bessel beam for LCP, due to the overlap of two beams. We

https://dx.doi.org/10.1021/acsphotonics.9b01608
ACS Photonics 2020, 7, 512–518

have performed numerical simulations on the multifunctional metalens (see section 3 in the Supporting Information). The simulation results are in good agreement with the experimental results presented in Figure 6.

CONCLUSION

In conclusion, we have developed a method to realize PSHE-based metalenses with multidimensional and multifunctional manipulation capabilities. First, we propose a PSHE-based metalens with different transverse split focal lines for LCP and RCP light. This metalens can work as an ultrathin polarization analyzer, allowing us to distinguish the polarization states of incident light by monitoring the transverse intensity difference in the focal plane. Second, using the same method we also design a metalens with different longitudinal focal lines for LCP and RCP light. Third, we demonstrate a multifunctional metalens acting as an axicon for LCP light and meanwhile a convex lens for RCP light. The three distinct metalenses confirm that our method is able to realize novel PSHE-based metalens with multifunctional and multidimensional light manipulation. It is worth noticing that the method developed here is suitable for one-dimensional or two-dimensional planar metalens, not only for metallic but also for dielectric metalens.[4,25,26,29] We believe that our approach provides a flexible way to design other spin-dependent meta-devices for a variety of potential applications, including polarimetric imaging, optical manipulation, holograms, and sensing.

ASSOCIATED CONTENT

Supporting Information

The Supporting Information is available free of charge at https://pubs.acs.org/doi/10.1021/acsphotonics.9b01608.

Simulation bandwidth of multidimensional metalens, efficiency of multidimensional metalens, and simulation results for multifunctional metalens (PDF)

AUTHOR INFORMATION

Corresponding Authors

Yongmin Liu − *Department of Mechanical and Industrial Engineering and Department of Electrical and Computer Engineering, Northeastern University, Boston, 02115, United States*; orcid.org/0000-0003-1084-6651; Email: y.liu@northeastern.edu

Zheng-Gao Dong − *Physics Department, Southeast University, Nanjing 211189, China*; Email: zgdong@seu.edu.cn

Authors

Renchao Jin − *Physics Department, Southeast University, Nanjing 211189, China*

Lili Tang − *Physics Department, Southeast University, Nanjing 211189, China*

Jiaqi Li − *Physics Department, Southeast University, Nanjing 211189, China*

Jin Wang − *Physics Department, Southeast University, Nanjing 211189, China*

Qianjin Wang − *National Laboratory of Solid State Microstructures, Nanjing University, Nanjing 210093, China*

Complete contact information is available at: https://pubs.acs.org/10.1021/acsphotonics.9b01608

Funding

This work was supported by the National Natural Science Foundation of China No. 11774053, Natural Science Foundation of Jiangsu Province of China (BK20181263). Y.L. acknowledges the financial support of National Science Foundation (ECCS-1916839).

Notes

The authors declare no competing financial interest.

REFERENCES

(1) Khorasaninejad, M.; Capasso, F. Metalenses: Versatile multifunctional photonic components. *Science* **2017**, *358*, eaam8100.

(2) Yu, N.; Genevet, P.; Kats, M. A.; Aieta, F.; Tetienne, J.-P.; Capasso, F.; Gaburro, Z. Light propagation with phase discontinuities: generalized laws of reflection and refraction. *Science* **2011**, *334*, 333−337.

(3) Dong, F.; Feng, H.; Xu, L.; Wang, B.; Song, Z.; Zhang, X.; Yan, L.; Li, X.; Tian, Y.; Wang, W.; Sun, L.; Li, Y.; Chu, W. Information Encoding with Optical Dielectric Metasurface via Independent Multichannels. *ACS Photonics* **2019**, *6*, 230−237.

(4) Mueller, J. P. B.; Rubin, N. A.; Devlin, R. C.; Groever, B.; Capasso, F. Metasurface polarization optics: independent phase control of arbitrary orthogonal states of polarization. *Phys. Rev. Lett.* **2017**, *118*, 11391.

(5) Jin, L.; Dong, Z.; Mei, S.; Yu, Y. F.; Wei, Z.; Pan, Z.; Rezaei, S. D.; Li, X.; Kuznetsov, A. I.; Kivshar, Y. S.; Yang, J. K. W.; Qiu, C.-W. Noninterleaved Metasurface for (2^6-1) Spin- and Wavelength-Encoded Holograms. *Nano Lett.* **2018**, *18*, 8016−8024.

(6) Zhang, Y.; Liu, W.; Gao, J.; Yang, X. Generating focused 3D perfect vortex beams by plasmonic metasurfaces. *Adv. Opt. Mater.* **2018**, *6*, 1701228.

(7) Wang, Y.; Wei, D.; Zhu, Y.; Huang, X.; Fang, X.; Zhong, W.; Wang, Q.; Zhang, Y.; Xiao, M. Conversion of the optical orbital angular momentum in a plasmon-assisted second-harmonic generation. *Appl. Phys. Lett.* **2016**, *109*, 081105.

(8) Khorasaninejad, M.; Chen, W. T.; Devlin, R. C.; Oh, J.; Zhu, A. Y.; Capasso, F. Metalenses at visible wavelengths: Diffraction-limited focusing and subwavelength resolution imaging. *Science* **2016**, *352*, 1190−1194.

(9) Chen, X.; Huang, L.; Muhlenbernd, H.; Li, G.; Bai, B.; Tan, Q.; Jin, G.; Qiu, C.-W.; Zhang, S.; Zentgraf, T. Dual-polarity plasmonic metalens for visible light. *Nat. Commun.* **2012**, *3*, 1198.

(10) Pors, A.; Nielsen, M. G.; Eriksen, R. L.; Bozhevolnyi, S. I. Broadband focusing flat mirrors based on plasmonic gradient metasurfaces. *Nano Lett.* **2013**, *13*, 829−834.

(11) Paniagua-Dominguez, R.; Yu, Y. F.; Khaidarov, E.; Choi, S.; Leong, V.; Bakker, R. M.; Liang, X.; Fu, Y. H.; Valuckas, V.; Krivitsky, L. A.; Kuznetsov, A. I. A metalens with a near-unity numerical aperture. *Nano Lett.* **2018**, *18*, 2124−2132.

(12) Chen, W. T.; Khorasaninejad, M.; Zhu, A. Y.; Oh, J.; Devlin, R. C.; Zaidi, A.; Capasso, F. Generation of wavelength-independent subwavelength Bessel beams using metasurfaces. *Light: Sci. Appl.* **2017**, *6*, e16259.

(13) Zhu, Y.; Wei, D.; Kuang, Z.; Wang, Q.; Wang, Y.; Huang, X.; Zhang, Y.; Xiao, M. Broadband variable meta-axicons based on nano-aperture arrays in a metallic film. *Sci. Rep.* **2018**, *8*, 11591.

(14) Boroviks, S.; Deshpande, R. A.; Mortensen, N. A.; Bozhevolnyi, S. I. Multifunctional metamirror: polarization splitting and focusing. *ACS Photonics* **2018**, *5*, 1648−1653.

(15) Arbabi, A.; Horie, Y.; Bagheri, M.; Faraon, A. Dielectric metasurfaces for complete control of phase and polarization with subwavelength spatial resolution and high transmission. *Nat. Nanotechnol.* **2015**, *10*, 937−943.

(16) Xu, H.-X.; Hu, G.; Han, L.; Jiang, M.; Huang, Y.; Li, Y.; Yang, X.; Ling, X.; Chen, L.; Zhao, J.; Qiu, C.-W. Chirality-Assisted High Efficiency Metasurfaces with Independent Control of Phase, Amplitude, and Polarization. *Adv. Opt. Mater.* **2018**, *7*, 1801479.

(17) Chen, W. T.; Zhu, A. Y.; Sanjeev, V.; Khorasaninejad, M.; Shi, Z.; Lee, E.; Capasso, F. A broadband achromatic metalens for focusing and imaging in the visible. *Nat. Nanotechnol.* **2018**, *13*, 220−226.
(18) Wang, S.; Wu, P. C.; Su, V. C.; Lai, Y. C.; Chen, M. K.; Kuo, H. Y.; Chen, B. H.; Chen, Y. H.; Huang, T. T.; Wang, J. H.; Lin, R. M.; Kuan, C. H.; Li, T.; Wang, Z.; Zhu, S.; Tsai, D. P. A broadband achromatic metalens in the visible. *Nat. Nanotechnol.* **2018**, *13*, 227−232.
(19) Yin, X.; Steinle, T.; Huang, L.; Taubner, T.; Wuttig, M.; Zentgraf, T.; Giessen, H. Beam switching and bifocal zoom lensing using active plasmonic metasurfaces. *Light: Sci. Appl.* **2017**, *6*, e17016.
(20) Chen, X.; Chen, M.; Mehmood, M. Q.; Wen, D.; Yue, F.; Qiu, C. W.; Zhang, S. Longitudinal multifoci metalens for circularly polarized light. *Adv. Opt. Mater.* **2015**, *3*, 1201−1206.
(21) Arbabi, E.; Li, J.; Hutchins, R. J.; Kamali, S. M.; Arbabi, A.; Horie, Y.; Van Dorpe, P.; Gradinaru, V.; Wagenaar, D. A.; Faraon, A. Two-photon microscopy with a double-wavelength metasurface objective lens. *Nano Lett.* **2018**, *18*, 4943−4948.
(22) Zhou, Y.; Kravchenko, I. I.; Wang, H.; Nolen, J. R.; Gu, G.; Valentine, J. Multilayer noninteracting dielectric metasurfaces for multiwavelength metaoptics. *Nano Lett.* **2018**, *18*, 7529−7537.
(23) Ma, W.; Huang, Z.; Bai, X.; Zhan, P.; Liu, Y. Dual-band light focusing using stacked graphene metasurfaces. *ACS Photonics* **2017**, *4*, 1770−1775.
(24) Ling, X.; Zhou, X.; Huang, K.; Liu, Y.; Qiu, C. W.; Luo, H.; Wen, S. Recent advances in the spin Hall effect of light. *Rep. Prog. Phys.* **2017**, *80*, 066401.
(25) Devlin, R. C.; Ambrosio, A.; Rubin, N. A.; Mueller, J. P. B.; Capasso, F. Arbitrary spin-to−orbital angular momentum conversion of light. *Science* **2017**, *358*, 896−901.
(26) Li, S.; Li, X.; Wang, G.; Liu, S.; Zhang, L.; Zeng, C.; Wang, L.; Sun, Q.; Zhao, W.; Zhang, W. Multidimensional Manipulation of Photonic Spin Hall Effect with a Single-Layer Dielectric Metasurface. *Adv. Opt. Mater.* **2019**, *7*, 1801365.
(27) Xu, H. X.; Han, L.; Li, Y.; Sun, Y.; Zhao, J.; Zhang, S.; Qiu, C. W. Completely spin-decoupled dual-phase hybrid metasurfaces for arbitrary wavefront control. *ACS Photonics* **2019**, *6*, 211−220.
(28) Xu, H. X.; Hu, G.; Li, Y.; Han, L.; Zhao, J.; Sun, Y.; Yuan, F.; Wang, G. M.; Jiang, Z. H.; Ling, X.; Cui, T. J.; Qiu, C. W. Interference-assisted kaleidoscopic meta-plexer for arbitrary spin-wavefront manipulation. *Light: Sci. Appl.* **2019**, *8*, 3.
(29) Ding, G.; Chen, K.; Luo, X.; Zhao, J.; Jiang, T.; Feng, Y. Dual-Helicity Decoupled Coding Metasurface for Independent Spin-to-Orbital Angular Momentum Conversion. *Phys. Rev. Appl.* **2019**, *11*, 044043.
(30) Yin, X.; Ye, Z.; Rho, J.; Wang, Y.; Zhang, X. Photonic spin Hall effect at metasurfaces. *Science* **2013**, *339*, 1405−1407.
(31) Ling, X.; Zhou, X.; Yi, X.; Shu, W.; Liu, Y.; Chen, S.; Luo, H.; Wen, S.; Fan, D. Giant photonic spin Hall effect in momentum space in a structured metamaterial with spatially varying birefringence. *Light: Sci. Appl.* **2015**, *4*, e290.
(32) Wang, Y. H.; Jin, R. C.; Li, J. Q.; Zhong, F.; Liu, H.; Kim, I.; Jo, Y.; Rho, J.; Dong, Z. G. Photonic spin Hall effect by the spin-orbit interaction in a metasurface with elliptical nano-structures. *Appl. Phys. Lett.* **2017**, *110*, 101908.
(33) Liu, Y.; Ling, X.; Yi, X.; Zhou, X.; Chen, S.; Ke, Y.; Luo, H.; Wen, S. Photonic spin Hall effect in dielectric metasurfaces with rotational symmetry breaking. *Opt. Lett.* **2015**, *40*, 756−759.
(34) Jiang, Q.; Bao, Y.; Lin, F.; Zhu, X.; Zhang, S.; Fang, Z. Spin-controlled integrated near-and far-field optical launcher. *Adv. Funct. Mater.* **2018**, *28*, 1705503.
(35) Ke, Y.; Liu, Y.; Zhou, J.; Liu, Y.; Luo, H.; Wen, S. Optical integration of Pancharatnam-Berry phase lens and dynamical phase lens. *Appl. Phys. Lett.* **2016**, *108*, 101102.
(36) Zhou, J.; Qian, H.; Hu, G.; Luo, H.; Wen, S.; Liu, Z. Broadband photonic spin Hall meta-lens. *ACS Nano* **2018**, *12*, 82−88.
(37) Wen, D.; Yue, F.; Kumar, S.; Ma, Y.; Chen, M.; Ren, X.; Kremer, P. E.; Gerardot, B. D.; Taghizadeh, M. R.; Buller, G. S.; Chen, X. Metasurface for characterization of the polarization state of light. *Opt. Express* **2015**, *23*, 10272−10281.
(38) Aieta, F.; Genevet, P.; Kats, M. A.; Yu, N.; Blanchard, R.; Gaburro, Z.; Capasso, F. Aberration-free ultrathin flat lenses and axicons at telecom wavelengths based on plasmonic metasurfaces. *Nano Lett.* **2012**, *12*, 4932−4936.

https://dx.doi.org/10.1021/acsphotonics.9b01608
ACS Photonics 2020, 7, 512−518